Coupling of discrete and continuum electronic states in atom-atom collisions: A coupled-channels investigation of Penning ionization in He*(1s2s,³S) + Ar

John C. Bellum* and David A. Micha

Quantum Theory Project, Departments of Physics and Chemistry, University of Florida, Gainesville, Florida 32611
(Received 28 January 1977)

Transitions among discrete and continuum electronic states of diatomics, induced by atom-atom collisions and leading to ionization, are described by rigorously making the continuous electron energies ϵ discrete. An expansion in functions of ϵ leads to a set of coupled-channel scattering equations which may be solved to obtain differential and integral cross sections per unit of electron energies. This procedure is applied to Penning ionization in He*(1s2s,³S) + Ar collisions by choosing a suitable expansion basis and numerically integrating a selected set of coupled equations. Results confirm the Franck-Condon nature of electron emission used in previous theoretical analyses. They were obtained with a parametrized exponential coupling potential between the states of HeAr* and HeAr⁺ + e⁻. The calculations include total integral cross sections per unit electron energies and the contribution of individual partial waves at a given final energy. These cross sections show prominent features that may be related to the potential of the product heavy particles.

I. INTRODUCTION

In this paper we address the problem of discrete and continuum electronic states in collision processes such as Penning and associative ionization (PI and AI) of an atom or molecule B due to energy transfer from an excited (metastable) atom A^*. Penning ionization and AI have been the focus of considerable experimental and theoretical interest.[1-8] An important feature distinguishing PI and AI from other chemi-ionization processes is that the excitation energy of A^* exceeds the ionization potential of B. This means that the internal electronic state of the quasimolecule formed during collision consists of a discrete state embedded in the continuum of electronic states associated with the free emitted electron in the presence of the bound electrons of the molecular ion after ionization. As a consequence, in quantum-mechanical investigations of the collision dynamics in PI and AI, the role played by such resonant electronic states and the related continuum electronic states becomes a matter of prime concern.

For the most part, quantum-mechanical treatments of PI and AI[9,10] have been cast in terms of well-known resonant-state formalisms.[11,12] These treatments focus on the width $\Gamma(R)$ which determines the rate of decay of a discrete state into the continuum at internuclear separation R. Within the context of such formalisms, various semi-classical and semiempirical approaches have been introduced, leading to theoretical results for total PI and AI cross sections,[13-27] angular distributions for elastic scattering,[24-29] and energy[15,19,27,30] and angular[31,32] distributions of emitted electrons. Reasonably good agreement with experimental measurements is usually obtained, at least within limited ranges of the collision energy E.

Owing to the very limited information available in the majority of cases regarding the R behavior of the $A^* + B$ and $A + B^+$ interaction potentials, as well as $\Gamma(R)$, these quantities have of necessity been represented in terms of parametrized functional forms in most theoretical treatments. Key parameters specifying the behaviors of the functions are determined by trying to bring calculated results into agreement with experimental results.[16-30] Such determinations are not always unique,[24] however, and often have been successful only by using potentials whose behaviors are described by piecing together several functional forms, each valid over a specific range of R.[19,22,24-29] As has been emphasized by Berry in a recent assessment of the theory,[6] there is a need for theoretical approaches which can successfully calculate measurable quantities, such as energy distributions of emitted electrons, to further constrain the potential parameters.

In keeping with this point of view, we have approached PI and AI within the framework of formal discretization procedures applied to the continuum of internal electronic states associated with these processes. The usefulness of such discretization techniques has been advanced previously by Bloch, who applied them to continua encountered in nuclear reactions,[33] and by Wolken, who applied them to gas-solid energy-transfer phenomena[34] and to collisional dissociation of diatomic molecules by atoms.[35]

In a previous report,[36] we outlined some of the main features of our present approach. In this paper it is our intention to make a more thorough presentation of our application of discretization theory to PI and AI. In Sec. II we review our

earlier theoretical considerations, and establish the formal framework provided by discretization of the continuum of internal electronic states. In Sec. III we discuss in detail physically reasonable approximations which were made within this framework, leading to the treatment of PI and AI in terms of a number of two-state coupled equations. Each set of two-state coupled equations describes the heavy-particle dynamics for ionization in which the emitted electron has kinetic energy ϵ within a given incremental range in the continuum of kinetic energies that it may carry away.

In Secs. IV–VI we expand the specific case of PI in He* $(1s2s, {}^3S)$ +Ar collisions. In Sec. IV we consider in detail the He*$(1s2s, {}^3S)$ +Ar and He +Ar${}^+(3p^5, {}^2P)$ interaction potentials, and discuss a convenient functional form for atom-atom potentials which represents them over the entire range of internuclear separations. In Sec. V the connection between the decay width $\Gamma(R)$ and the coupling matrix elements between discrete and continuum electronic states is used to make reasonable estimates of the latter based on semiempirical parameterizations of $\Gamma(R)$.

In Sec. VI we report new results from calculations for PI of Ar by He*$(1s2s, {}^3S)$, and describe some computational details. Refined calculations of partial ionization cross sections per unit energy ϵ of the emitted electron confirm our previously reported results, showing an ϵ dependence in good agreement with experimentally measured energy distributions of emitted electrons, and further showing more structural detail of the distributions. Partial cross-section contributions for the heavy particles in specific angular momentum states are also singled out. Their behavior as a function of ϵ, or of the angular-momentum partial wave number, shows structure which reflects regions of high density of states in the continuum of final relative motion of the heavy particles.

II. THEORETICAL FRAMEWORK

The continuum electronic states in PI and AI can be characterized as those associated with an electron escaping the region of the molecule along a direction specified by the unit vector $\hat{e}$ [in body-fixed (BF), center of mass of the nuclei frame]. The electrons escape with an amount of kinetic energy ϵ which is constrained by conservation of total energy during the collision. The continuum state of the emitted electron can be well represented outside the atomic cores by an appropriate linear combination of Coulomb wave functions. Designating the continuum state of the emitted electron by $\phi^c_{\epsilon,\hat{e}}(\vec{r})$, one can write

$$\phi^c_{\epsilon,\hat{e}}(\vec{r}) = \sum_{\lambda\mu} {}' Y^*_{\lambda\mu}(\hat{e}) \phi^c_{\epsilon\lambda\mu}(\vec{r}), \tag{1}$$

where $\phi^c_{\epsilon\lambda\mu}(\vec{r})$ is a Coulomb wave function of energy ϵ with angular momentum quantum numbers λ and μ in the BF frame. That is,[37]

$$\phi^c_{\epsilon\lambda\mu}(\vec{r}) = R_{\epsilon\lambda}(r) Y_{\lambda\mu}(\hat{r}), \tag{2}$$

where the asymptotic behavior of the radial function $R_{\epsilon\lambda}(r)$ is

$$R_{\epsilon\lambda}(r) \underset{r\to\infty}{\sim} \left(\frac{2}{\pi k}\right)^{1/2}$$

$$\times \frac{\sin[kr + \delta_\lambda + \sigma_\lambda - \frac{1}{2}\lambda\pi + (1/k)\ln(2kr)]}{r}. \tag{3}$$

In this expression $k = \sqrt{2\epsilon}$ is the wave number of the emitted electron in atomic units, σ_λ is the Coulomb phase shift of the λth Coulomb partial wave, and δ_λ is the phase shift arising from the remaining potential. The continuum orbitals of Eq. (1) are normalized to unity on the energy scale, meaning

$$\langle \phi^c_{\epsilon,\hat{e}} | \phi^c_{\epsilon',\hat{e}'} \rangle = \delta(\epsilon - \epsilon')\delta(\hat{e} - \hat{e}'), \tag{4}$$

where the brackets indicate integration over the electronic coordinates.

In a many-electron description of the interaction between a discrete electronic state and the continuum of electronic states in which it is embedded, the primary mechanism for transition to the continuum is configuration interaction among the states.[12] In an earlier paper[38] we discussed PI and AI on the basis of molecular-orbital correlation diagrams and showed that these processes are of the Auger-type,[39] involving two-electron transitions mediated by Coulomb interactions. Born-Oppenheimer couplings, due to the influence of the heavy-particle motions on the electronic structure, need not be considered except at very short internuclear distances. Hence, it appears appropriate to describe PI and AI by means of diabatic discrete and continuum electronic states, which couple through the electronic Hamiltonian. Furthermore, it has been found[31,32,38] that relatively few λ-partial waves contribute to the states of emitted electrons, with $\lambda = 0$ dominating in the case of He* +Ar. Electronic angular momenta can in this case be neglected compared to nuclear angular momenta.

We turn next to the heavy-particle dynamics, and expand the total wave function of electrons and nuclei at each R in terms of a complete set containing both discrete and continuum electronic states $\{\Phi_n\}$ and $\{\Phi_\epsilon\}$, respectively. If n_i is the discrete-state label of the incident channel, then the wave function with outgoing

waves may accordingly be expressed as

$$\Psi_{n_i}^{(+)}(\vec{R}, \vec{X}) = \frac{1}{R} \sum_{LM} Y_{LM}(\hat{R})$$

$$\times \left(\sum_n \Phi_n(\vec{R}, \vec{X})\Psi_{nn_i}^{LM}(R) \right.$$

$$\left. + \int_0^\infty d\epsilon \Phi_\epsilon(\vec{R}, \vec{X})\Psi_{\epsilon n_i}^{LM}(R) \right). \quad (5)$$

Here $\vec{X}$ indicates all of the electronic coordinates and the sum over (LM) results from a partial wave decomposition associated with the angular momentum states of the nuclei. In the usual fashion, Eq. (5) is substituted into the Schrödinger equation $H\Psi_{n_i}^{(+)} = E\Psi_{n_i}^{(+)}$, where E is the total energy (i.e., collision energy) for the colliding atoms, and $H = -(1/2m)\nabla_R^2 + H_{el}$ is the Hamiltonian comprised of the nuclear kinetic energy $-(1/2m)\nabla_R^2$ and the electronic Hamiltonian H_{el}. Here atomic units are used, m is the reduced mass of the nuclei, and H_{el} includes the nuclear-nuclear electrostatic repulsion. The Schrödinger equation results in the following continuously infinite set of coupled equations (independent of the superscript M),

$$\left(\frac{1}{2m}\frac{d^2}{dR^2} - \frac{L(L+1)}{2mR^2} + E \right)\Psi_{nn'}^L(R)$$

$$\quad (6a)$$

$$= \sum_p V_{np}(R)\Psi_{pn'}^L(R) + \int_0^\infty d\epsilon\, V_{n\epsilon}(R)\Psi_{\epsilon n'}^L(R),$$

$$\left(\frac{1}{2m}\frac{d^2}{dR^2} - \frac{L(L+1)}{2mR^2} + E \right)\Psi_{\epsilon'n'}^L(R)$$

$$\quad (6b)$$

$$= \sum_n V_{\epsilon'n}(R)\Psi_{nn'}^L(R) + \int_0^\infty d\epsilon\, V_{\epsilon'\epsilon}(R)\Psi_{\epsilon n'}^L(R),$$

where, for example, $V_{n\epsilon} = \langle \Phi_n |H_{el}| \Phi_\epsilon \rangle$ is a Coulomb coupling matrix element. These sets of coupled equations determine (with the proper boundary conditions for scattering) the expansion coefficients $\Psi_{nn'}^L(R)$ and $\Psi_{\epsilon n'}^L(R)$ associated, respectively, with $n \rightarrow n'$ and $\epsilon \rightarrow n'$ transitions during collision.

In order for these coupled equations to be of any practical use, not only must the set of electronic states (which in principle is infinite) be kept small, but also the terms of Eq. (6) involving integration over the energy ϵ of the emitted electron must be suitably reduced to a tractable form. This we have accomplished by means of discretization of the continuum, whereby the heavy-particle wave functions associated with transitions into the continuum are formally expanded in a complete set $\{a_I(\epsilon)\}$ of discrete functions of the continuum variable ϵ:

$$\Psi_{\epsilon n}^L(R) = \sum_{I=1}^\infty a_I(\epsilon)\Psi_{In}^L(R). \quad (7)$$

The set of functions $\{a_I(\epsilon)\}$ are taken to obey the completeness relations,

$$\sum_{I=1}^\infty a_I^*(\epsilon)a_I(\epsilon') = \delta(\epsilon - \epsilon'), \quad (8a)$$

$$\int_0^\infty d\epsilon\, a_I^*(\epsilon)a_J(\epsilon) = \delta_{IJ}. \quad (8b)$$

The use of Eq. (7) in Eq. (6) leads to the following modified set of (discretized) coupled equations:

$$\left(\frac{1}{2m}\frac{d^2}{dR^2} - \frac{L(L+1)}{2mR^2} + E \right)\Psi_{nn'}^L(R)$$

$$= \sum_p V_{np}(R)\Psi_{pn'}^L(R) + \sum_I V_{nI}(R)\Psi_{In'}^L(R), \quad (9a)$$

$$\left(\frac{1}{2m}\frac{d^2}{dR^2} - \frac{L(L+1)}{2mR^2} + E \right)\Psi_{In}^L(R)$$

$$= \sum_p V_{Ip}(R)\Psi_{pn}^L(R) + \sum_J V_{IJ}(R)\Psi_{Jn}^L(R), \quad (9b)$$

where

$$V_{nI}(R) = \int_0^\infty d\epsilon\, V_{n\epsilon}(R)a_I(\epsilon), \quad (10a)$$

$$V_{In}(R) = V_{nI}^*(R), \quad (10b)$$

$$V_{IJ}(R) = \int_0^\infty d\epsilon' \int_0^\infty d\epsilon\, a_I^*(\epsilon') V_{\epsilon'\epsilon}(R)a_J(\epsilon). \quad (10c)$$

Equations (9a) and (9b) may be combined into a single set of coupled equations corresponding to scattering in a set of effective electronic states which span both discrete and continuum parts of electronic configuration space. We simply introduce a label α which ranges over the combined discrete labels n and I. Then Eqs. (9a) and (9b) can be written as a single matrix equation,

$$\underline{D_R^L}\underline{\Psi}^L(R) = \underline{V}(R)\underline{\Psi}^L(R), \quad (11)$$

where the matrices are defined as follows:

$$\underline{D_R^L} = \left[\left(\frac{1}{2m}\frac{d^2}{dR^2} - \frac{L(L+1)}{2mR^2} + E \right)\delta_{\alpha\alpha'} \right], \quad (12a)$$

$$\underline{V}(R) = [V_{\alpha\alpha'}(R)], \quad (12b)$$

$$\underline{\Psi}^L(R) = [\Psi_{\alpha\alpha'}^L(R)]. \quad (12c)$$

The desired physical solutions of Eq. (11) must fulfill scattering boundary conditions. In what follows, only so-called open channels of the heavy-particle motion are considered, with wave number k_α given by

$$(1/2m)k_\alpha^2 = \lim_{R\to\infty} \{E - V_{\alpha\alpha}(R)\} > 0.$$

The scattering boundary conditions may be expressed in terms of the Ricatti-Bessel and -Neumann functions $\mu_L(x)$ and $\nu_L(x)$, respectively, as well as $w_L^{(+)}(x) = \nu_L(x) + i\mu_L(x)$. The boundary conditions are then written

$$\Psi_{\alpha\alpha'}^{L}(R) \underset{R \to 0}{\sim} 0, \tag{13a}$$

$$\Psi_{\alpha\alpha'}^{L}(R) \underset{R \to \infty}{\sim} \mu_L(k_\alpha R)\delta_{\alpha\alpha'}$$

$$+ w_L^{(+)}(k_\alpha R)\left(\frac{k_{\alpha'}}{k_\alpha}\right)^{1/2} T_{\alpha\alpha'}^{L}. \tag{13b}$$

The asymptotic conditions can be summarized by introducing the matrices

$$\underline{I}_L^{(s)}(R) = [\delta_{\alpha\alpha'} k_\alpha^{-1/2} \mu_L(k_\alpha R)], \tag{14a}$$

$$\underline{I}_L^{(c)}(R) = [\delta_{\alpha\alpha'} k_\alpha^{-1/2} \nu_L(k_\alpha R)], \tag{14b}$$

$$\underline{I}_L^{(\pm)}(R) = \underline{I}_L^{(c)}(R) \pm i\underline{I}_L^{(s)}(R), \tag{14c}$$

so that Eq. (13b) corresponds to

$$\underline{\Psi}^{L}(R) \underset{R \to \infty}{\sim} \{\underline{I}_L^{(s)}(R) + \underline{I}_L^{(+)}(R)\underline{T}^{L}\}\underline{k}^{1/2}, \tag{15}$$

where

$$\underline{T}^{L} = (T_{\alpha\alpha'}^{L}), \tag{16a}$$

$$\underline{k} = (\delta_{\alpha\alpha'} k_\alpha). \tag{16b}$$

In practice the physical solution to Eq. (11) [satisfying the boundary conditions of Eq. (13)] can be obtained as a linear combination of linearly independent (column vector) solutions, $\underline{Y}_1^{L}$, $\underline{Y}_2^{L}$, ... which satisfy Eq. (11) with the boundary condition of Eq. (13a). Upon integrating the full matrix $\underline{Y}^{L}$ of these linearly independent solutions into the asymptotic region we obtain matrices $\underline{A}^{L}$ and $\underline{B}^{L}$ according to the scattering-boundary conditions,

$$\underline{Y}^{L}(R) \underset{R \to \infty}{\sim} \underline{I}_L^{(s)}(R)\underline{A}^{L} - \underline{I}_L^{(c)}(R)\underline{B}^{L}. \tag{17}$$

The R matrix of coupled-channel theory can be calculated as

$$\underline{R}^{L} = \underline{B}^{L}(\underline{A}^{L})^{-1}, \tag{18}$$

from which S and T matrices are obtained in the form

$$\underline{S}^{L} = (\underline{1} + i\underline{R}^{L})(\underline{1} - i\underline{R}^{L})^{-1}, \tag{19a}$$

$$\underline{T}^{L} = -\tfrac{1}{2} i(\underline{S}^{L} - \underline{1}). \tag{19b}$$

The S- and T-matrix elements for our physical process are determined as the appropriate linear combinations, based on Eq. (7), of the S- and T-matrix elements for transition from a discrete state to a discretized continuum state.[35] That is,

$$S_{\epsilon n}^{L} = \sum_{I} S_{In}^{L} a_I(\epsilon), \tag{20a}$$

$$T_{\epsilon n}^{L} = \sum_{I} T_{In}^{L} a_I(\epsilon). \tag{20b}$$

Finally, cross sections (per unit energy) for transition from a discrete state to a continuum

state are given by the expression,

$$\frac{d\sigma_{\epsilon \leftarrow n}(E, \epsilon)}{d\epsilon} = \left(\frac{4\pi}{k_n^2}\right) \sum_{L} (2L+1)|T_{\epsilon n}^{L}|^2. \tag{21}$$

In concluding this summary of the discretization formalism, we would like to emphasize that it constitutes a rigorous approach applicable in general to collisions involving coupling between discrete and continuum electronic states, of which PI and AI are just representative examples.

III. DISCRETIZATION IN PI AND AI PROCESSES

The basic features of PI and AI can be studied in terms of a single discrete diatomic potential labeled by V_1, embedded in an energy continuum associated with a potential V_2 for the diatomic ion plus an emitted electron with energy ϵ. This is illustrated in Fig. 1, which shows the actual interaction potentials we used for $He^*(1s2s, {}^3S)$ $+Ar$. V_{12} is the coupling potential, and $E_f(R)$ the final relative energy of the heavy particles when
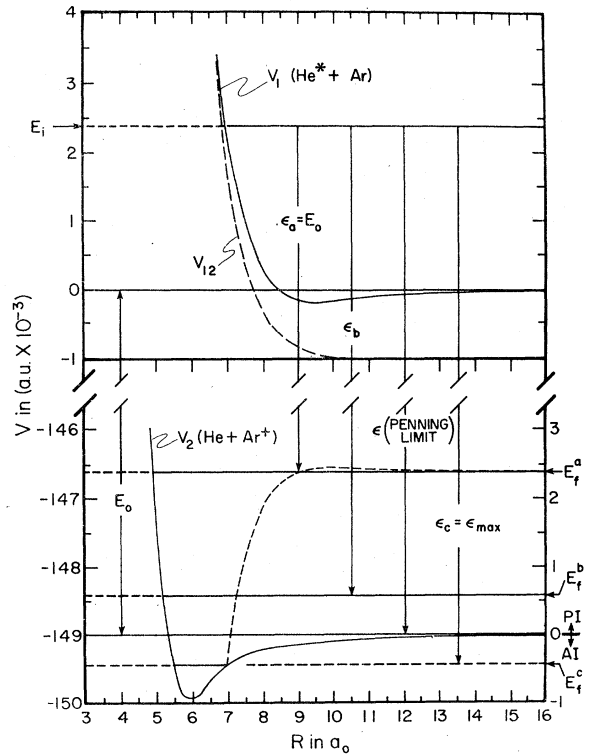

FIG. 1. Potentials and coupling for PI and AI of Ar by $H^*(1s2s, {}^3S)$. V_1 and V_2 label, respectively, the potentials for $He^*(1s2s, {}^3S) + Ar$ and $He + Ar^+$ $(3p^5, {}^2P)$. V_{12} labels a typical coupling matrix element (referred to the left scale shifted by 10^{-3} a.u.). E_i labels a typical (thermal) collision energy, and the lower dotted curve shows $E_f(R)$ for Franck-Condon transitions, as discussed in the text. E_0, the energy difference between the separated limits of V_1 and V_2, is indicated.

the electron emission is of the Franck-Condon type and the initial relative energy is E_i. A simple, but physically reasonable, set of discrete functions of the continuum variable ϵ is introduced. Namely, the set of functions $\{a_I(\epsilon)\}$ used in the expansion of Eq. (7) is taken to be a set of step functions in ϵ as follows:

$$a_I(\epsilon) = \begin{cases} (\Delta\epsilon)^{-1/2} & \text{for } \epsilon_I - \tfrac{1}{2}\Delta\epsilon \leqslant \epsilon \leqslant \epsilon_I + \tfrac{1}{2}\Delta\epsilon, \\ 0 & \text{otherwise}. \end{cases} \quad (22)$$

This choice of basis functions divides the ϵ scale into increments of size $\Delta\epsilon$, where the Ith such increment is centered about $\epsilon_I = (I - \tfrac{1}{2})\Delta\epsilon$. The basis set of step functions only partially satisfies the completeness relations of Eq. (8). That is,

$$\int_0^\infty d\epsilon\, a_I^*(\epsilon) a_J(\epsilon) = \delta_{IJ} \quad (23)$$

and

$$\sum_I a_I^*(\epsilon) a_I(\epsilon') = \begin{cases} 1/\Delta\epsilon & \text{for } \epsilon \text{ and } \epsilon' \text{ both in the} \\ & \text{same increment } J, \\ 0 & \text{otherwise}. \end{cases} \quad (24)$$

In terms of this step-function basis set the modified coupling terms of Eq. (10) (with d now labeling the discrete state) are expressed as

$$V_{dI}(R) = (\Delta\epsilon)^{-1/2} \int_{\epsilon_I - \Delta\epsilon/2}^{\epsilon_I + \Delta\epsilon/2} d\epsilon \langle \Phi_d | H_{el} | \Phi_\epsilon \rangle, \quad (25a)$$

$$V_{Id}(R) = V_{dI}^*(R), \quad (25b)$$

$$V_{IJ}(R) = (\Delta\epsilon)^{-1} \int_{\epsilon_I - \Delta\epsilon/2}^{\epsilon_I + \Delta\epsilon/2} d\epsilon' \int_{\epsilon_J - \Delta\epsilon/2}^{\epsilon_J + \Delta\epsilon/2} d\epsilon$$

$$\times \langle \Phi_{\epsilon'} | H_{el} | \Phi_\epsilon \rangle. \quad (25c)$$

These coupling-matrix elements may be obtained, if the increment $\Delta\epsilon$ is made small enough, from, e.g.,

$$(\Delta\epsilon)^{-1/2} \int_{\epsilon_I - \Delta\epsilon/2}^{\epsilon_I + \Delta\epsilon/2} d\epsilon \langle \Phi_d | H_{el} | \Phi_\epsilon \rangle$$

$$\simeq (\Delta\epsilon)^{1/2} \langle \Phi_d | H_{el} | \Phi_{\epsilon_I} \rangle. \quad (26)$$

As has been mentioned, the continuum electronic states here are those of an emitted electron in the presence of a single bound state of the molecular ion. If $\vec{r}_c$ locates the continuum electron, then, for $r_c \to \infty$, one may make the following approximation:

$$H_{el}(R, \vec{X})\Phi_\epsilon(R, \vec{X}_{N-1}, r_c \to \infty)$$

$$\simeq [V^+(R) + \epsilon]\Phi_\epsilon(R, \vec{X}_{N-1}, r_c \to \infty), \quad (27)$$

or

$$\langle \Phi_{\epsilon'} | H_{el} | \Phi_\epsilon \rangle \simeq [V^+(R) + \epsilon']\delta(\epsilon - \epsilon'). \quad (28)$$

Here $V^+(R)$ is the interaction potential of the molecular ion (designated by V_2 in Fig. 1), and $\vec{X}_{N-1}$ denotes the coordinates of the $N-1$ remaining electrons. This approximation amounts to neglecting coupling between continuum electronic states. In view of the fact that the continuum electronic states in PI and AI describe very energetic emitted electrons[5,7,40-42] escaping the region of the molecular ion quickly, the approximation of Eq. (28) is a reasonable one. On the basis of Eq. (28), and for $\Delta\epsilon$ small, the matrix elements V_{IJ} in Eq. (25c) can be expressed as

$$V_{IJ}(R) \simeq (\Delta\epsilon)^{-1} \int_{\epsilon_I - \Delta\epsilon/2}^{\epsilon_I + \Delta\epsilon/2} d\epsilon'$$

$$\times \int_{\epsilon_J - \Delta\epsilon/2}^{\epsilon_J + \Delta\epsilon/2} d\epsilon [V^+(R) + \epsilon']\delta(\epsilon' - \epsilon)$$

$$\simeq [V^+(R) + \epsilon_I]\delta_{IJ}. \quad (29)$$

With these approximations, the coupled equations of Eq. (9) reduce to

$$\left(\frac{1}{2m} \frac{d^2}{dR^2} - \frac{L(L+1)}{2mR^2} + E - V_{dd}(R) \right) \Psi_{dd}^L(R)$$

$$= \sum_I (\Delta\epsilon)^{1/2} \langle \Phi_d | H_{el} | \Phi_{\epsilon_I} \rangle \Psi_{Id}^L(R), \quad (30a)$$

$$\left(\frac{1}{2m} \frac{d^2}{dR^2} - \frac{L(L+1)}{2mR^2} + E - V^+(R) - \epsilon_I \right) \Psi_{Id}^L(R)$$

$$= (\Delta\epsilon)^{1/2} \langle \Phi_{\epsilon_I} | H_{el} | \Phi_d \rangle \Psi_{dd}^L(R). \quad (30b)$$

In Eq. (30a) $V_{dd}(R) = \langle \Phi_d | H_{el} | \Phi_d \rangle$, and is the interaction potential of the discrete state which we mentioned previously and labeled V_1 in Fig. 1. The present coupled-channels approach makes no assumptions about Franck-Condon transitions, and therefore includes no a priori restrictions on the range of ϵ values. Rather, the coupled-channels calculations themselves assess the range of dynamically important ϵ values.

Equation (30) is analogous to the coupled-channel equations of scattering for discrete target states, a consequence of having introduced a discretization before writing down transition amplitudes, instead of afterwards as is customary. A succession of increasingly approximate procedures may now be followed. For the $I \to d$ transition we can keep only two coupled equations from the set (the standard two-state approximation of coupled-channels theory), which accounts for the (Id) coupling to all orders. In this way the collision dynamics of PI and AI is treated in terms of N sets of two-channel coupled equations. Each set of two-channel coupled equations results from Eq. (30)

by including only the $J = I$ term in the sum of Eq. (30a), and corresponds to transition into some Ith discretized continuum state. Such a set of coupled equations can be solved for the solutions which satisfy scattering-boundary-conditions, exactly as described in Sec. II. As a result, R, S, and T matrices are found for each $I-d$ transition according to Eqs. (18) and (19), and $\epsilon - d$ cross sections are calculated from Eqs. (20) and (21) specialized to the step-function basis of Eq. (22).

Distorted-wave approximations[10,27] could also be obtained in our approach by further uncoupling our two-channel equations. In this connection it is worth pointing out that our equations do not contain the imaginary term $-\frac{1}{2}i\Gamma$ added to V_{dd}, because transitions of the type $d - I - d$ (which the imaginary term would represent) are already included in our two coupled equations, insofar as the (Id) coupling is included to all orders. The present approach is in fact an alternative to the use of complex potentials.

IV. INTERACTION POTENTIALS FOR He*(1s2s,³S) + Ar PI AND AI COLLISIONS

A primary consideration in representing an interaction potential is that of joining the short-range repulsion to the long-range van der Waals attraction in a way which adequately describes the region of the potential minimum. As mentioned in the Introduction, the approach often taken is to splice together, from one region to the next, potential functions appropriate for each region.[19,22,24-29] A single potential function valid over the entire range of R, however, is both convenient and desirable. In this connection, Lennard-Jones (12-6) potentials have been used for the interaction potential of the metastable state.[43] From studies of collisional ionization of Ar by Ne*,[17] however, it appears that the Lennard-Jones (12-6) potential is too repulsive, which would be of steadily worsening consequence as the collision energy increases. The same has been found for a Lennard-Jones (12-6) potential in the case of He* +Ar collisions.[18] On the other hand, Morse potentials which yield suitable potential well depths and positions tend to produce repulsions which are too soft.[18,25,27] As a result, in a recent study of He* (1s2s, ³S) +Ar collisions,[25] several repulsive behaviors were spliced together to obtain good agreement with angular distributions for elastic scattering over a fairly wide range of collision energies.

In view of these results, it appears that a major problem in representing interaction potentials for PI and AI centers around describing the repulsive behavior. In the cases of He* +Ar and He +Ar⁺,

we have carried out non-spin-polarized $MSX\alpha$ calculations of the electronic structure as a function of R.[38] The $MSX\alpha$ total energies as a function of R for these calculations show the typical Born-Mayer (BM) repulsion dependence $Ae^{-R/b}$, for $2.3a_0 \leqslant R \leqslant 10.0a_0$ in the case of He* +Ar, and for $2.0a_0 \leqslant R \leqslant 6.0a_0$ in the case of He +Ar⁺. Such BM repulsion was also found in our earlier $MSX\alpha$ calculations of some rare-gas diatoms in their ground states,[44] where total energies were overestimated, but where the b parameters were of reasonable magnitude. So, on the basis of our $MSX\alpha$ calculations,[38] it appears that a BM repulsion is quite adequate for both He* +Ar and He +Ar⁺ interaction potentials. Therefore, we have determined BM b parameters from our calculations for He* +Ar and He +Ar⁺ [38] according to the same procedure described for the ground-state rare-gas diatom results.[44]

Toennies has found that a reasonable potential function for atoms is one obtained simply by adding together a BM repulsion and a van der Waals attraction potential.[45] In our work, we introduced a similar potential function, but one in which the long-range van der Waals attractive potential (which has, for instance, R^{-4}, R^{-6}, R^{-8}, etc., behavior) is smoothly suppressed at small R.

A function well suited for such a suppression is the one studied by Eckart[46] to simulate potential-energy barriers

$$f_E(R; R_o, \beta, B) = (1 + e^{-(R-R_o)/B})^{-1}$$
$$\times [1 + \beta(1 + e^{(R-R_o)/B})^{-1}]. \quad (31)$$

As can be seen, $f_E \to 1$, for $R \gg R_o$, $f_E \to 0$ exponentially for $R \ll R_o$, and f_E exhibits a local maximum at R_{max} for $\beta > 0$ given by

$$(R_{max} - R_o)/B = \ln[(\beta+1)/(\beta-1)]. \quad (32)$$

Denoting by $V_{lr}(R)$ the long-range van der Waals attractive potential, we introduced the following potential function:

$$V(R) = Ae^{-R/b} + V_{lr}(R)f_E(R; R_o, \beta, B). \quad (33)$$

This function can be applied to both the He* (1s2s, ³S) +Ar and He +Ar⁺(3p⁵, ²P) potentials. We choose the position R_{max} of the local maximum of f_E to coincide with R_m, the position of the minimum of $V(R)$. We can thus determine R_o by Eq. (32). The BM b parameter in Eq. (33) is taken from our $MSX\alpha$ calculations, carried out for Σ states of HeAr* and HeAr⁺. Since the BM b parameter reflects the "softness" or "hardness" of the repulsion,[44] we use it also to determine the exponential behavior of the Eckart function. That is, we take $B = b$. Finally, the BM A parameter and the Eckart β parameter are determined by the potential-well

conditions,

$$V(R_m) = -\epsilon_m, \tag{34a}$$

$$dV(R)/dR|_{R_m} = 0, \tag{34b}$$

where ϵ_m is the well depth.

For He*(1s2s, ^3S) +Ar, the values for R_m and ϵ_m we use are those found by Chen, Haberland, and Lee[19] in an analysis of their measured angular distributions for elastic He* +Ar collisions. Their He* +Ar potential has been the one most reliably determined until the recent work of Wang, Hickman, Shobatake, and Lee.[24] The He* +Ar potential of Wang et al., however, has about the same well depth as reported by Chen et al., with an R_m shifted to somewhat larger R. So both sets of (R_m, ϵ_m) parameters can be considered to be reasonably valid for the purpose of testing our theoretical approach. The C_6 coefficient we use for He* +Ar is the one reported by Bell, Dalgarno, and Kingston.[47]

Potentials for He +Ar$^+$ have been determined from data on the ratio of AI to PI cross sections, together with considerations of energy balance based on Franck-Condon transitions.[19,20] Recently Nakamura has reanalyzed the experimental data within a semiempirical framework, and proposed a new He +Ar$^+$ potential.[22] We use the R_m and ϵ_m values for Nakamura's He +Ar$^+$ potential as well as his value for the C_6 coefficient based on the Slater-Kirkwood formula in terms of the polarizabilities of He and Ar$^+$. The He +Ar$^+$ C_4 coefficient we use is the accurate (experimental) value quoted by Dalgarno.[48]

Table I summarizes the parameters we use for the He*(1s2s, ^3S) +Ar and He +Ar$^+$(3p^5, ^2P) interaction potentials. The potentials themselves are the ones shown in Fig. 1. Regarding the BM b parameters we point out that our value for He* +Ar is nearly twice that reported for Li and Ar,[49] which was the value used by Olson[18] as a guideline for the He* +Ar repulsion. For He +Ar$^+$, our value of b (0.532a_0) is quite close to the one we calculated for He +Ar (0.5435a_0),[44] which supports the idea that He +Ar and He +Ar$^+$ share similar repulsive behavior.

Figure 2 displays the interaction potential for He*(1s2s, ^3S) +Ar represented by Eq. (33) with the parameters of Table I. The various contributing terms of Eq. (33) are shown explicitly. We draw attention in particular to the deviation from R^{-6} behavior of the long-range portion of the potential modulated by the Eckart function, as well as to the Eckart function itself. For clarity, the Eckart function has been plotted against an arbitrary scale. As can be seen, comparison with the Morse-Spline—van der Waals potential of Chen

TABLE I. Parameters for the interaction potentials of He*(1s2s, ^3S) + Ar and He + Ar*(3p^5, ^2P) as given by Eq. (33), where $B=b$ and R_0 is given by Eq. (32) with R_{max} =R_m. β and B are determined by Eq. (34). The b parameters are from MSXα calculations (Ref. 38).

	He*+Ar	He+Ar*
A (a.u.)	4.39678	44.6527
b (a_0)	0.9675	0.532
ϵ_m (a.u)	0.1583×10^{-3} [a]	0.945×10^{-3} [c]
$R_m (a_0)$	9.4488 [a]	5.936 [c]
C_6 (a.u.)$(a_0)^6$	226.0 [b]	7.94 [c]
C_4 (a.u)$(a_0)^4$	...	0.6904 [d]
β	2.81505	6.42317

[a] Chen et al. (Ref. 19).   [c] Nakamura (Ref. 22).
[b] Bell et al. (Ref. 47).   [d] Dalgarno (Ref. 48).

et al.[19] is quite good. The Eckart form matches their well-depth parameters with slightly stronger repulsion than provided by the Morse potential, and slightly less attraction in the region just beyond the potential minimum.

Figure 3 is a similar plot for He +Ar$^+$, contrasting our potential, according to Eq. (33) and Table I, with the one proposed by Nakamura.[22] Nakamura's potential joins two functional forms describing different regions of R. Again, the comparison is good, the Eckart form showing slightly weaker repulsion, and first less and then more attraction for R beyond the potential minimum.[50]
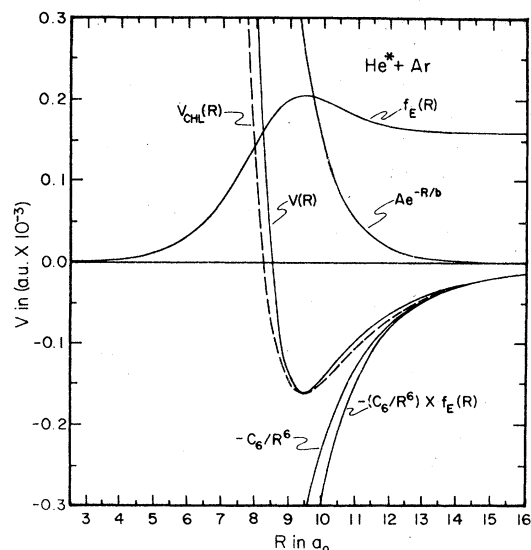

FIG. 2. $V(R)$ of Eq. (33) for He*(1s2s, ^3S) +Ar with the parameters of Table I. The various contributions to $V(R)$ are indicated. $V_{CHL}(R)$ labels the corresponding potential proposed by Chen, Haberland, and Lee (Ref. 19), shown for comparison. The Eckart function $f_E(R)$ is plotted against an arbitrary scale for clarity.
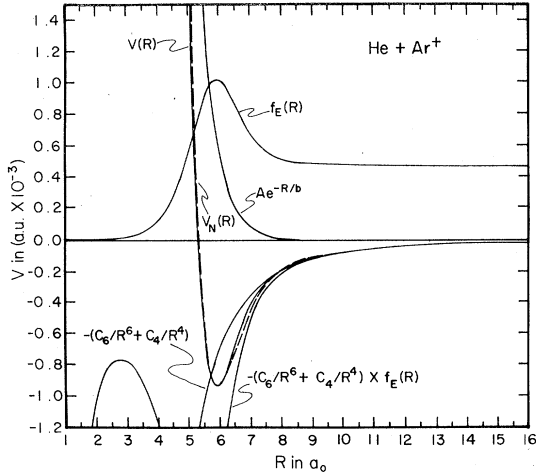
FIG. 3. $V(R)$ of Eq. (33) for $\text{He}+\text{Ar}^+$ $(3p^5, {}^2P)$ with the parameters of Table I. The various contributions to $V(R)$ are indicated. $V_N(R)$ labels the corresponding potential proposed by Nakamura (Ref. 22), shown for comparison. The Eckart function $f_E(R)$ is plotted against an arbitrary scale for clarity.

V. PARAMETRIZATION OF THE COUPLING

The potentials we have just proposed provided suitably parametrized expressions for $V_{dd}(R)$ and $V^+(R)$ appearing in Eq. (30). The remaining expressions required to solve these coupled equations are the Coulomb coupling matrix elements $(\Delta\epsilon)^{1/2}\langle\Phi_d|H_{el}|\Phi_{\epsilon_I}\rangle$. We will rely on functional forms which have been used in semiempirical and other quantum-mechanical approaches to represent the decay width $\Gamma(R)$.

The decay width can be expressed as[9,10]

$$\Gamma(R) = 2\pi|\langle\Phi_d|H_{el}|\Phi_\epsilon\rangle|^2 , \quad (35)$$

where Φ_d is a discrete state and Φ_ϵ is a continuum state degenerate with Φ_d. In other theoretical approaches to PI and AI in $\text{He}^*({}^3S)+\text{Ar}$ collisions, parameterizations for $\Gamma(R)$ have been proposed[18,20-22,24,25,27] based on a simple exponential representation,

$$\Gamma(R) = A_\Gamma e^{-R/a_\Gamma} . \quad (36)$$

This functional form appears to represent $\Gamma(R)$ quite well based on both experimental and theoretical analysis.[5]

Equations (35) and (36) suggest that the coupling-matrix element itself may be expressed in simple exponential form. In addition, the range of parameters A_Γ and a_Γ determined in various semiempirical analyses should provide good guidelines for choosing reasonable parameters for an exponential form of the coupling matrix element.

Now the matrix element $\langle\Phi_d|H_{el}|\Phi_\epsilon\rangle$ has ϵ as well as R dependence. In most treatments of $\Gamma(R)$,

however, a lack of information prevents explicit consideration of the ϵ dependence. Thus, when A_Γ and a_Γ are adjusted to give semiempirical results in agreement with experiment, they reflect primarily the behavior of $\Gamma(R)$ at an energy ϵ_0 near the most probable energy of the emitted electron (i.e., the peak of the electron-energy distribution). Clearly, since each set of two-channel coupled equations holds for a particular incremental range of the ϵ scale, it would be desirable to have coupling matrix elements reflecting appropriate ϵ dependence.

We assess this ϵ dependence in terms of the ϵ dependence of the continuum orbital describing the emitted electron. Reference to Eq. (3) shows that a continuum orbital of energy ϵ, described according to Eq. (1), has dominant asymptotic ϵ dependence in the factor $\sqrt{2/\pi k} = \sqrt{2/\pi}/(\sqrt{2\epsilon})^{1/2}$ associated with the density of Coulomb states. Its other ϵ dependence, appearing in the argument of the sine function, should be weak since the sine function remains bound by ± 1 regardless of its argument. Although the region of configuration space near the molecule (where the emitted electrons see more than simply a Coulomb field) contributes to $\langle\Phi_d|H_{el}|\Phi_\epsilon\rangle$, because the emitted electrons are energetic, and their state oscillates rapidly at short distances, we expect the ϵ dependence of $\langle\Phi_d|H_{el}|\Phi_\epsilon\rangle$ to be well described on the basis of Eq. (3).

Therefore, for each continuum state Φ_ϵ we introduce a state $\tilde{\Phi}_\epsilon$ given by

$$\Phi_\epsilon = [\sqrt{2/\pi}/(\sqrt{2\epsilon})^{1/2}]\tilde{\Phi}_\epsilon . \quad (37)$$

We further write

$$\langle\Phi_d|H_{el}|\Phi_\epsilon\rangle$$

$$= [\sqrt{2/\pi}/(\sqrt{2\epsilon})^{1/2}]\langle\Phi_d|H_{el}|\tilde{\Phi}_\epsilon\rangle , \quad (38)$$

and expect the matrix element on the right-hand side of the equation to have only weak ϵ dependence. It is the R dependence of this matrix element we express in exponential form:

$$\langle\Phi_d|H_{el}|\tilde{\Phi}_\epsilon\rangle = A_m e^{-R/a_m} . \quad (39)$$

Relying on Eqs. (35), (36), (38), and (39), and using a value ϵ_0 near the peak of the emitted electron-energy distribution, we arrive at the appropriate expression relating A_m and a_m to A_Γ and a_Γ:

$$A_\Gamma e^{-R/a_\Gamma} = (4/\sqrt{2\epsilon_0})A_m^2 e^{-2R/a_m} . \quad (40)$$

Recalling that $A_m e^{-R/a_m}$ expresses the weak ϵ-dependent part of a coupling matrix element, we write the couplings of Eq. (30):

$$(\Delta\epsilon)^{1/2}\langle\Phi_d|H_{el}|\Phi_{\epsilon_I}\rangle$$

$$\simeq (\Delta\epsilon)^{1/2}[\sqrt{2/\pi}/(\sqrt{2\epsilon_I})^{1/2}]A_m e^{-R/a_m} . \quad (41)$$

For PI and AI in $He^*(1s2s, {}^3S)$ +Ar collisions, typical values of the emitted electron energy are around 0.1505 a.u..[7,19,51] This is the value we use for ϵ_0 in Eq. (40) to compute A_m and a_m values based on A_Γ and a_Γ as determined in several semi-empirical analyses. As the results in Table II show, there is a wide range of A_m and a_m values indicated by semiempirical calculations. The values based on Olson's work[18] deviate markedly from the others. Olson, however, chose to vary only the exponential factor a_Γ in his work, leaving $A_\Gamma = 1.0$ a.u. Basically the trends set by semiempirical work indicate an a_m value of about $0.7a_0$ and A_m values in the range 20–100 a.u.

VI. RESULTS FROM COUPLED-CHANNELS CALCULATIONS FOR PI OF Ar BY $He^*(1s2s, {}^3S)$

The potentials and couplings of Secs. IV and V provided us the necessary quantities for applying the treatment of PI presented in Secs. II and III to the case of PI in $He^*(1s2s, {}^3S)$ +Ar collisions. From now on we refer to the $He^*(1s2s, {}^3S)$ +Ar potential as V_1, and the $He + Ar^+(3p^5, {}^2P)$ potential as V_2, as shown in Fig. 1. Accordingly, for some lth increment of the ϵ scale, the two-channel coupled equations are solved, as discussed in Sec. II, by integrating two linearly independent solutions into the asymptotic region. We carried out such calculations by implementing a coupled-channels computer program which performs the numerical integration using the de Vogelaere algorithm.[52] In the asymptotic region R-, S-, and T-matrix elements were calculated for $I \rightarrow d$ transitions by matching to scattering boundary conditions according to Eqs. (18) and (19). Then, for ϵ in the lth increment, the S- and T-matrix elements for $\epsilon \rightarrow d$ transitions were calculated according to Eq. (20), and the partial ionization cross section per unit energy of the emitted electron according to Eq. (21).

We introduced a convenient criterion for determining both integration starting points R_s and initial solution derivatives D simultaneously,[53] by estimating the starting solutions in terms of JWKB

functions. Upon inspecting Fig. 1, one sees that the repulsive wall of V_1 is probed roughly in the range $5.6a_0$–$8.0a_0$ for typical initial-collision energies, whereas the repulsive wall of V_2 is probed roughly in the range $4.5a_0$–$5.5a_0$ for corresponding final-collision energies. Consequently, an R_s appropriate for V_2 will nearly always be too deep inside the repulsive wall of V_1. Whether R_s and D values were determined by our criterion, or some other suitable means, the integration over the several extra Bohr radii in the classically forbidden region of V_1 led to numerically excessive increases of the corresponding solution components. We found that a successful way to circumvent these numerical difficulties is to suppress the problematic solution components governed by V_1 deep inside its nonclassical region.[53]

At the time of our earlier report[36] we had performed calculations for $\Delta\epsilon = 2 \times 10^{-4}$ a.u. with coupling parameters $A_m = 50.0$ a.u. and $a_m = 0.7a_0$. As Table II shows, these coupling parameters are roughly midway in the range of values extracted from semiempirical work. With these same A_m and a_m parameters we have extended our earlier calculations by a refinement of the increment to $\Delta\epsilon = 1 \times 10^{-4}$ a.u. over a portion of the ϵ scale.

Figure 4 displays the results of calculations of $d\sigma_{\epsilon \leftarrow d}(E, \epsilon)/d\epsilon$ as a function of ϵ. As before,[36] a smooth curve has been drawn through the $d\sigma_{\epsilon \leftarrow d}(E, \epsilon)/d\epsilon$ values at the midpoints of the increments along the ϵ scale. The bottom scale shows the final collision energy $E_f = E + E_0 - \epsilon$ of the heavy-particle motion corresponding to each energy ϵ of the emitted electrons, and the top scale shows ϵ referenced to E_0 (see Fig. 1). The limit for PI lies at the right-hand edge of Fig. 4. The plot would be continued further to the right for the AI distribution. Since we have so far treated just the open-channel boundary conditions of Sec. II, our calculations are for PI only, and extend to the last increment before entering the AI region. An extension of the calculations to the AI region, where closed-channel boundary conditions are required, is presently being implemented. For the

TABLE II. A_Γ and a_Γ values of Eq. (36) reported in several semiempirical analyses as indicated and the A_m and a_m values of Eq. (41) calculated by Eq. (40) with $\epsilon_0 = 0.1505$ a.u.

Semiempirical analysis	A_Γ (a.u.)	$a_\Gamma (a_0)$	A_m (a.u.)	$a_m (a_0)$
Pesnelle et al.[a]	4000.0	0.36	23.41	0.72
Illenberger and Niehaus[b]	7400.0	0.357	31.85	0.714
Nakamura[c]	73 000.0	0.34	100.00	0.68
Olson[d]	1.0	0.667	1.0	1.334

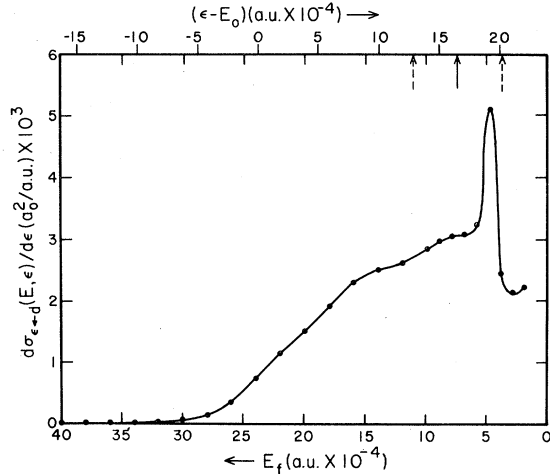[a] From Ref. 20.
[b] From Ref. 21.
[c] From Ref. 22.
[d] From Ref. 18.

FIG. 4. Partial ionization cross section per unit
energy of the emitted electron calculated for PI of Ar
by He*($1s2s$, ^3S) at an incident collision energy E
$=23.89\times10^{-4}$ a.u. ($\simeq 65$ meV), and plotted as described
in the text. For these calculations, $\Delta\epsilon=2\times10^{-4}$ a.u.
for $E_f>10\times10^{-4}$ a.u. and 1×10^{-4} a.u. for $E_f\leqslant10\times10^{-4}$
a.u.

results of Fig. 4, $\Delta\epsilon=2\times10^{-4}$ a.u. for $E_f>10$
$\times10^{-4}$ a.u. and $\Delta\epsilon=1\times10^{-4}$ a.u. for $E_f\leqslant10\times10^{-4}$
a.u.

From Fig. 4 we see some of the important fea-
tures of our coupled-channels approach to the
collision dynamics. In particular, cross-section
contributions from incremental regions for $\epsilon<E_0$
diminish abruptly, as they should on the basis of
purely qualitative considerations in terms of
Franck-Condon transitions. The distribution we
calculate is indeed confined to the very narrow
range of ϵ found experimentally.[5,7,51] In addition,
although we make no Franck-Condon assumptions
in our approach, we calculate a distribution which
peaks for $\epsilon>E_0$, in keeping with the predominance
of Franck-Condon-type transitions.

As we pointed out before,[36] an interesting com-
parison can be made with experimental PI electron-
energy distributions reported by Hotop.[7] He shows
distributions measured at collision energies of 36,
95, and 125 meV. The peaks of these three dis-
tributions, in order of increasing collision energy,
shift in roughly linear fashion to higher ϵ, being
located at ($\epsilon-E_0$) values of about 35, 55, and 70
meV, respectively. Our results are for $E=65$
meV, which is nearly midway between 36 and 95
meV. So, based on the trends shown by the experi-
mental results of Hotop,[7] the peak of our distribu-
tion should fall approximately between the peaks
at 36 and 95 meV. Along the top edge of Fig. 4
we have indicated by the left dashed arrow the
experimental peak for $E=36$ meV, and by the
right dashed arrow the experimental peak for

$E=95$ meV. The solid arrow is drawn midway be-
tween the two dashed arrows. The calculated dis-
tribution does peak roughly between the two ex-
perimental peaks, as expected, though it tends to
favor ϵ values to the right of the solid arrow.
This behavior is more evident now than before,[36]
since, by refinement of $\Delta\epsilon$ to 1×10^{-4} a.u. for
$E_f<10\times10^{-4}$ a.u., we have resolved the sharp
peak of the distribution located at $E_f\simeq5\times10^{-4}$ a.u.
Preliminary calculations made in the region of
the pronounced peak using even more refined $\Delta\epsilon$
values[54] indicate that its sharp structure persists
and additional smaller structure becomes re-
solved. It remains to be seen whether these fea-
tures of electron distributions are smoothed out by
thermal averaging in the experiments, or whether
they would change in more refined theoretical
treatments.

Of interest in the study of the dynamics of the
heavy-particle motion are the L-partial cross
sections per unit energy of the emitted electron.
These are the terms which contribute to $d\sigma_{\epsilon\leftarrow d}(E,$
$\epsilon)/d\epsilon$ according to Eq. (21). For the $\Delta\epsilon$ interval
where the sharp peak in Fig. 4 occurs, we ana-
lyzed $d\sigma_{\epsilon\leftarrow d}(E,\epsilon)/d\epsilon$ in terms of the L-partial cross
sections $d\sigma^L_{\epsilon\leftarrow d}(E,\epsilon)/d\epsilon$ and found that more than
half (i.e., $\simeq 2.81\times10^3a_0^2$/a.u.) of $d\sigma_{\epsilon\leftarrow d}(E,\epsilon)/d\epsilon$ is
contributed by the $L=24$ partial cross section. In-
spection of the $L=24$ effective potentials, $V_1^{(24)}$ and
$V_2^{(24)}$, together with the initial and final collision
energies, E and E_f, respectively, gives useful in-
sight into the possible reasons for such a large
contribution from $d\sigma^{(24)}_{\epsilon\leftarrow d}(E,\epsilon)/d\epsilon$. The situation
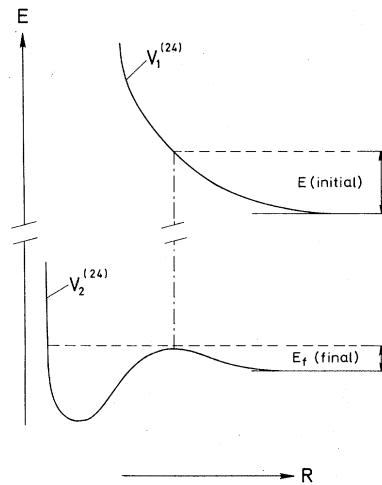we discovered is shown schematically in Fig. 5.

FIG. 5. Schematic diagram, patterned after Fig. 1,
of the $L=24$ effective V_1 and V_2 potentials, and initial
and final collision energies of 23.89×10^{-4} a.u. and 5.0
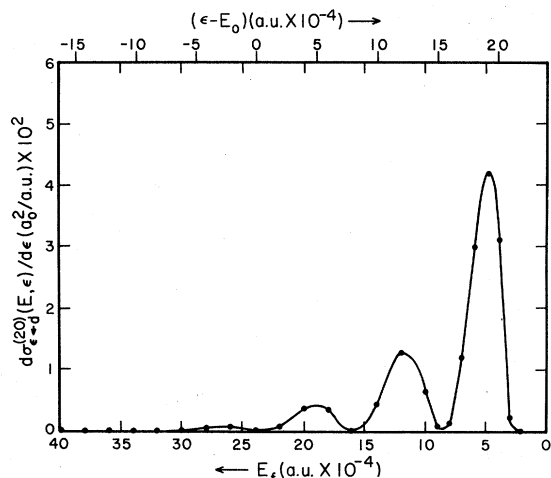$\times10^{-4}$ a.u., respectively.

FIG. 6. L-partial cross section per unit energy of the emitted electron [from Eq. (21)] for the $L = 20$ angular momentum component of the heavy particles, calculated for PI of Ar by He*$(1s2s, {}^3S)$ at an incident collision energy of $E = 23.89 \times 10^{-4}$ a.u. ($\simeq 65$ meV). The details of the plot are otherwise the same as for Fig. 4.
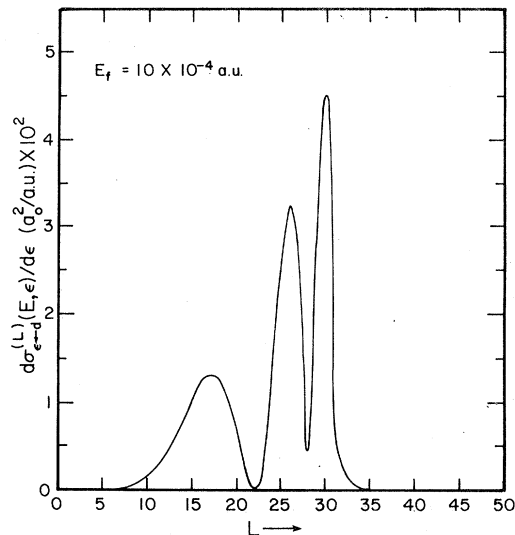

FIG. 7. L-partial cross section per unit energy of the emitted electron [from Eq. (21)] calculated for PI of Ar by He*$(1s2s, {}^3S)$ at an incident collision energy $E = 23.89 \times 10^{-4}$ a.u. ($\simeq 65$ meV), and plotted against the partial wave number L, for the final energy $E_f = E + E_0 - \epsilon$ indicated in the figure.

Namely, the classical turning point of $V_1^{(24)}$ falls in the neighborhood of the centripetal barrier of $V_2^{(24)}$, and the barrier height is very near the final collision energy $E_f = 5 \times 10^{-4}$ a.u., where the sharp peak of Fig. 4 occurs. This, of course, could account for such a large resonance behavior, owing to the

simultaneous combination of a typically high probability for transition at the classical turning point of the incident channel and a high likelihood of orbiting resonances in the final channel.

Further interesting studies can be made by looking at the behavior of $d\sigma_{\epsilon \leftarrow d}^{(L)}(E, \epsilon)/d\epsilon$ as a func-
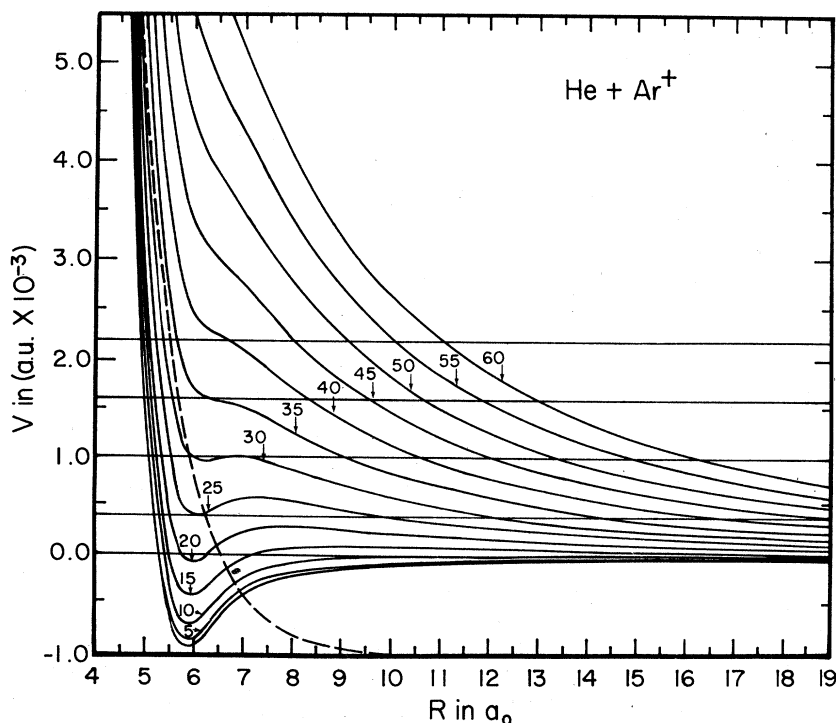

FIG. 8. Effective potentials $V_2^{(L)}$ for L-partial wave components of the heavy-particle angular momentum as indicated. The unlabeled curve is V_2 shown in Fig. 1. The dotted curve is a typical coupling matrix element, as shown in Fig. 1.

tion of ϵ for fixed L, and as a function of L for fixed interval along the ϵ scale. Figure 6 shows a plot, similar in all respects to Fig. 1, of $d\sigma^{(20)}_{\epsilon\leftarrow d}(E, \epsilon)/d\epsilon$. In our earlier report[36] the $L=20$ partial cross section was shown from calculations with $\Delta\epsilon = 2 \times 10^{-4}$ a.u. In Fig. 6, as in Fig. 4, the results for $E_f < 10 \times 10^{-4}$ a.u. are for a refined $\Delta\epsilon$ of 1×10^{-4} a.u. We see that the refined calculations resolve the large peak of contribution near $E_f = 5 \times 10^{-4}$ a.u. more sharply. As we pointed out earlier,[36] the structure of $d\sigma^{(20)}_{\epsilon\leftarrow d}(E, \epsilon)/d\epsilon$ exhibited in Fig. 6 shows successive resonance peaks of cross-section contribution which appear to reflect regions of high density of states in the continuum of final relative motion of the heavy particles having angular-momentum partial wave $L=20$.

Figure 7 shows a plot of $d\sigma^{(L)}_{\epsilon\leftarrow d}(E, \epsilon)/d\epsilon$ as a function of L for an interval centered on an ϵ value corresponding to the indicated E_f value. Again, pronounced resonance peaks of cross-section contribution are observed. This structure can be interpreted on the basis of Fig. 8, which displays effective potentials $V_2^{(L)}$ for $L = 0, 5, 10, \ldots$, etc.

Several final-channel energies E_f are indicated by the horizontal lines. Focusing attention on a single final-channel energy $(E_f = 10 \times 10^{-4}$ a.u. in the case of Fig. 7), one can see that, as L increases from 0, the specified channel energy will fall near resonance peaks (of the sort seen in Fig. 6) for some of the effective potentials $V_2^{(L)}$, and fall between such resonance peaks for other effective potentials. This would account for the resonance structure of Fig. 7.

*Present address: Fachbereich Physik, Universität Kaiserslautern, Postfach 3049, D–6750 Kaiserslautern, W. Germany.

[1] E. E. Muschlitz, Jr., Adv. Chem. Phys. 10, 171 (1966).

[2] E. E. Muschlitz, Jr., Science 159, 599 (1968).

[3] R. S. Berry, in *Molecular Beams and Reaction Kinetics*, edited by Ch. Schlier (Academic, New York, 1970), p. 193; Rec. Chem. Prog. 31, 9 (1970).

[4] R. D. Rundel and R. F. Stebbings, in *Case Studies in Atomic Collision Physics II*, edited by E. W. McDaniel and M. R. C. McDowell (North-Holland, Amsterdam, 1972), p. 549.

[5] A. Niehaus, Ber. Bunsenges. Phys. Chem. 77, 632 (1973).

[6] R. S. Berry, Radiat. Res. 59, 367 (1974).

[7] H. Hotop, Radiat. Res. 59, 379 (1974).

[8] C. Manus, Physica 82C, 165 (1976).

[9] H. Nakamura, J. Phys. Soc. Jpn. 26, 1473 (1969).

[10] W. H. Miller, J. Chem. Phys. 52, 3563 (1970).

[11] H. Feshbach, Ann. Phys. (N.Y.) 5, 357 (1958); 19, 287 (1962).

[12] U. Fano, Phys. Rev. 124, 1866 (1961).

[13] H. Fujii, H. Nakamura, and M. Mori, J. Phys. Soc. Jpn. 29, 1030 (1970).

[14] H. Nakamura, J. Phys. Soc. Jpn. 31, 574 (1971).

[15] W. H. Miller, C. A. Slocomb, and H. F. Schaefer, III, J. Chem. Phys. 56, 1347 (1972).

[16] D. A. Micha, S. Y. Tang, and E. E. Muschlitz, Jr., Chem. Phys. Lett. 8, 587 (1971).

[17] R. E. Olson, Chem. Phys. Lett. 13, 307 (1972).

[18] R. E. Olson, Phys. Rev. A 6, 1031 (1972).

[19] C. H. Chen, H. Haberland, and Y. T. Lee, J. Chem. Phys. 61, 3095 (1974).

[20] A. Pesnelle, G. Watel, and C. Manus, J. Chem. Phys. 62, 3590 (1975).

[21] E. Illenberger and A. Niehaus, Z. Phys. B 20, 33 (1975).

[22] H. Nakamura, J. Phys. B 8, L489 (1975).

[23] H. Nakamura, J. Phys. B 9, L1 (1976).

[24] Z. F. Wang, A. P. Hickman, K. Shobatake, and Y. T. Lee, J. Chem. Phys. 65, 1250 (1976).

[25] B. Brutschy, H. Haberland, and K. Schmidt, J. Phys. B 9, 2693 (1976).

[26] H. Haberland and K. Schmidt, J. Phys. B 10, 695 (1977).

[27] A. P. Hickman and H. Morgner, J. Phys. B 9, 1765 (1976).

[28] H. Haberland, C. H. Chen, and Y. T. Lee, in *Atomic Physics*, edited by S. J. Smith and G. K. Walters (Plenum, New York, 1973), Vol. 3, p. 339.

[29] B. Brutschy, H. Haberland, H. Morgner, and K. Schmidt, Phys. Rev. Lett. 36, 1299 (1976).

[30] R. J. Bieniek, J. Phys. B 7, L266 (1974); Chem. Phys. Lett. 40, 72 (1976).

[31] T. Ebding and A. Niehaus, Z. Phys. 270, 43 (1974).

[32] D. A. Micha and H. Nakamura, Phys. Rev. A 11, 1988 (1975).

[33] C. Bloch, in *Many-Body Description of Nuclear Structure and Reactions, Proceedings of the International School of Physics "Enrico Fermi," Course XXXVI*, edited by C. Bloch (Academic, New York, 1966), p. 394ff.

[34] G. Wolken, Jr., J. Chem. Phys. 60, 2210 (1974).

[35] G. Wolken, Jr., J. Chem. Phys. 63, 528 (1975).

[36] J. C. Bellum and D. A. Micha, Chem. Phys. 20, 121 (1977).

[37] See, for instance, K. C. Kulander and J. S. Dahler, J. Phys. B 8, 460 (1975), as well as Ref. 15.

[38] J. C. Bellum and D. A. Micha, Phys. Rev. A 15, 635 (1977).

[39] H. Hotop and A. Niehaus, Z. Phys. 228, 68 (1969).

[40] H. Hotop and A. Niehaus, Z. Phys. 238, 452 (1970).

[41]H. Hotop, G. Hübler, and L. Kaufhold, Int. J. Mass Spectrom. Ion Phys. **17**, 163 (1975).

[42]V. Čermák and J. B. Ozenne, Int. J. Mass Spectrom. Ion Phys. **7**, 399 (1971).

[43]E. W. Rothe, R.H. Neynaber, and S. M. Trujillo, J. Chem. Phys. **42**, 3310 (1965).

[44]J. C. Bellum and D. A. Micha, Int. J. Quantum Chem. Symp. **S8**, 229 (1974).

[45]J. P. Toennies, Chem. Phys. Lett. **20**, 238 (1973).

[46]C. Eckart, Phys. Rev. **35**, 1303 (1930).

[47]K. L. Bell, A. Dalgarno, and A. E. Kingston, J. Phys. B **1**, 18 (1968).

[48]A. Dalgarno, Adv. Phys. **11**, 281 (1962).

[49]A. A. Abrahamson, Phys. Rev. **178**, 76 (1969).

[50]The concave curve at the lower left of Fig. 3 is part of the Eckart-modulated long-range term. This be-
havior is due to the fact that the Eckart function does not approach zero strongly enough to quench the R^{-4} and R^{-6} terms as $R \rightarrow 0$. This is not crucial for the interaction potential, since it occurs only at very small R values. Equation (33) is valid over the dynamically important range of R, and the Eckart function has its primary importance in the region around R_m.

[51]H. Hotop, A. Niehaus, and A. L. Schmeltekopf, Z. Phys. **229**, 1 (1969).

[52]R. de Vogelaere, J. Res. Natl. Bur. Stand. **54**, 119 (1955).

[53]J. C. Bellum, Ph.D. dissertation (University of Florida, 1976) (unpublished).

[54]L. R. Relyea, J. C. Bellum, and D. A. Micha (unpublished).